Advanced Composite Materials
Publication details, including instructions for authors and subscription information:
http://www.tandfonline.com/loi/tacm20

In situ void content measurements during resin transfer molding

Ryosuke Matsuzaki [a] , Daigo Seto [b] , Akira Todoroki [b] & Yoshihiro Mizutani [b]

[a] Department of Mechanical Engineering , Tokyo University of Science , 2641 Yamazaki, Noda, Chiba , 278-8510 , Japan

[b] Department of Mechanical Sciences and Engineering , Tokyo Institute of Technology , 2-12-1 O-okayama, Meguro, Tokyo , 152-8552 , Japan

Published online: 22 May 2013.

To cite this article: Ryosuke Matsuzaki , Daigo Seto , Akira Todoroki & Yoshihiro Mizutani (2013) In situ void content measurements during resin transfer molding, Advanced Composite Materials, 22:4, 239-254, DOI: 10.1080/09243046.2013.801822

To link to this article: http://dx.doi.org/10.1080/09243046.2013.801822

Advanced Composite Materials, 2013
Vol. 22, No. 4, 239–254, http://dx.doi.org/10.1080/09243046.2013.801822

In situ void content measurements during resin transfer molding

Ryosuke Matsuzaki[a]*, Daigo Seto[b], Akira Todoroki[b] and Yoshihiro Mizutani[b]

[a]*Department of Mechanical Engineering, Tokyo University of Science, 2641 Yamazaki, Noda, Chiba 278-8510, Japan;* [b]*Department of Mechanical Sciences and Engineering, Tokyo Institute of Technology, 2-12-1 O-okayama, Meguro, Tokyo 152-8552, Japan*

(*Received 26 December 2012; accepted 30 April 2013*)

In resin transfer molding (RTM), the void content measured after resin curing does not represent the amount of voids at the point of air-trapping. To properly verify a prediction model for the void content based on the occurrence of voids due to the air-trapping mechanism, the void content must be measured immediately at the point of air-trapping. In the present study, we created an in situ method for measuring the void content during resin impregnation by combining image analysis with a technique that visualizes the resin flow and void formation during one-dimensional RTM. Using this proposed method, we measured changes in the distribution of the void content at the air-trapping site and following resin curing. As a result, an inversion phenomenon was observed, in which the void content decreased a short distance from the resin inlet due to the time that elapsed, whereas it increased at a longer distance. This phenomenon can be explained by the ease with which the void moved and by the effect of molecular diffusion. In addition, by measuring the change in void content during the time that elapsed from air-trapping until resin curing, we clarified the behavior of the void change and the factors that affect the void content following void formation.

Keywords: resin transfer molding; void; visualization; impregnation; resin cure; glass fiber; polyester resin

1. Introduction

Resin transfer molding (RTM) is a process that facilitates reduced manufacturing and material costs because it does not require the use of an expensive autoclave and prepregs.[1] However, owing to the complex microstructures of the woven fabric as well as the stochastic variation in the fabric alignment, the configuration of the flow front tends to be complicated, which often leads to the formation of voids. Because these voids that remain in the structure degrade the property of composites,[1] the application of RTM is currently limited to parts that do not require high reliability. In order for RTM to be more widely employed, it is essential to understand the mechanism of void generation and suppression in the process.[2]

Voids formed during RTM are classified as macro-, meso-, and micro-voids, depending on their scale. Macro-voids, which are also called dry spots, are large-scale voids that are formed by incomplete resin filling, and they are cured in an unimpregnated state.[3] Meso- and micro-voids, on the other hand, are very small bubbles that are

*Corresponding author. Email: rmatsuza@rs.tus.ac.jp

generated by air trapped at the flow front because of the largely microscopic structure of the fiber material. Meso-scale voids are voids that are trapped between fiber bundles, whereas micro-voids are inside a bundle.[4–7] Because even trace amounts of meso- or micro-voids significantly reduce the mechanical properties of the molded parts and are hard to suppress,[8–10] the present study focuses on understanding the mechanisms that govern their formation. In this paper, we use the single word 'void' to refer to both meso- and micro-voids.

In a conventional quantitative evaluation of void content, small specimens are usually cut from molded parts after resin curing. The void content is then measured by cross-sectional observation using a microscope, a combustion method, buoyancy measurements in water, or non-destructive testing using an ultrasonic C-scan. Cross-sectional observation using a microscope, which is usually combined with image analysis, enables us to measure the area of the void content and also to identify the shape and the location of the voids. In the combustion method, one measures the specimen's weight before and after removal of the resin from the test piece by combustion and then calculating the resulting difference from the theoretical weight under the assumption of a void-free material. In buoyancy measurement, a comparison is made between the weight of a specimen in air and in water.[1,11]

In past studies investigating the relationship between voids and the process parameters of resin impregnation, the void content measured after impregnation by any of these methods was used to evaluate the formation of voids at the flow front. [4,6,7,12–14] Schell et al. [14], for example, constructed a model for predicting void content based on the mechanism of air-trapping and demonstrated the validity of the model using the void content as measured by a micro-CT scan following resin curing.

However, voids trapped at the flow front during resin impregnation do not necessarily remain in molded parts without undergoing any change in volume. It is expected that there may be downstream movement of voids due to the macroscopic pressure differential, a volume change in voids due to pressure changes around the resin, or due to shrinkage during curing. Indeed, it has been reported that voids are moved along with the flow of resin following void formation.[4,15–17] We thus can see that the void content measured after resin curing does not represent the amount of voids that are formed at the point of air-trapping. Although the final goal of the study is to construct an analytical model to predict the void content of cured structures, precise analytical modeling of the void trapping is inevitable. To properly verify the model for predicting void content based on void formation due to the trapping mechanism, measuring the void content immediately at the point of air-trapping is necessary. After the void-trapping model is constructed, the effects of void transportation, surrounding pressure change, and cure shrinkage are then modeled to predict the final voidage.

In the present study, we propose a method of in situ measurement of the void content formed at the flow front in combination with image analysis and the visualization of voids and flow front during resin impregnation. In addition, using the proposed method, we investigate the change between the distribution of void contents when measured at the point of air-trapping and after resin curing. We also discuss the factors affecting the void content prior to the curing stage, based on microscopic observation of voids over elapsed time from the formation of voids to the completion of curing.

2. In situ quantitative method for evaluating void content

2.1. *Flow front visualization*

To evaluate the relationship between the flow velocity and the void content, one-dimensional flow experiments were conducted and the flow front and voids during the resin impregnation process were visualized. Because the optical refraction index of polymer resin and glass fibers is substantially equal, a fiber bundle impregnated with a resin has a transparent quality. Therefore, a fiber bundle impregnated with resin looks as if it disappears with the irradiation of diffused light; at this point, the interface between the resin and air, or the outlines of the flow front and voids can be clearly observed.

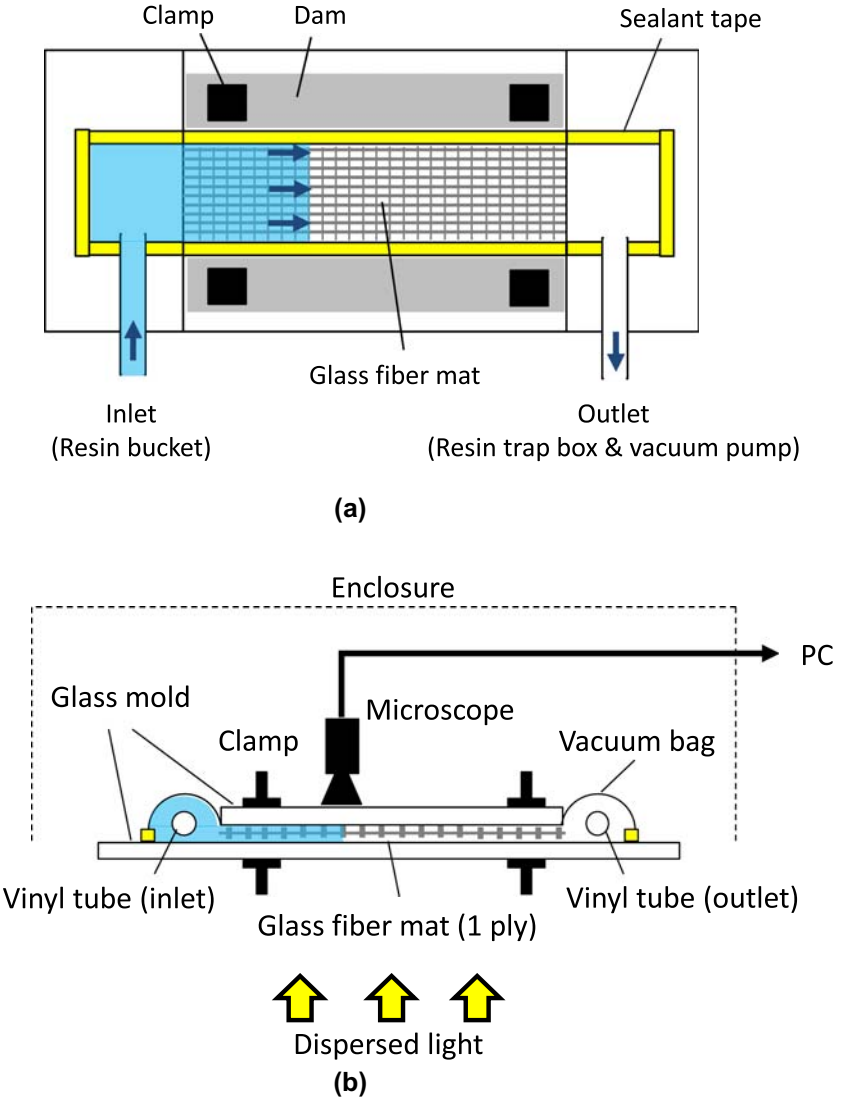

Figure 1. Experimental setup for flow front and void visualization during one-dimensional RTM; (a) upper view, (b) side view.

Figure 1 shows the experimental apparatus used for the visualization of the flow front and voids during the one-dimensional flow experiments. One layer of a rectangular plain woven glass fiber fabric was sandwiched between two colorless transparent glass plate molds. Both longitudinal sides of the glass fabrics were sealed with sealant tape and then fixed between glass plate molds by using clamps through insertion of glass composite dams. Negative pressure was applied at the flow front using a vacuum pump and was controlled using a vacuum regulator (NVR200-01-GB, Koganei). The diffused light was irradiated from the lower surface of the mold during resin impregnation. A digital microscope (M3, Scholar) was installed on the upper surface of the mold and was then connected to a PC. The entire apparatus was covered with a thin black cloth to reduce the reflection from the surrounding light source, as shown in Figure 1(b). Figure 2 shows a typical flow front that was observed in these one-dimensional flow experiments. Figure 3 shows a microscopic image of the flow front and voids that were observed using the proposed visualization method, in which both the flow front and the voids can be clearly observed. Because the fiber bundles seem to disappear owing to their impregnation with resin, the void content can be easily calculated via image analysis.

2.2. Measurements of void content by image analysis

To quantitatively evaluate the amount of voids, the area where voids were present was measured via image analysis by using the image of the voids acquired by the visualization method presented in Section 2.1. Figure 4 shows a flow chart of the void content measurements obtained by image analysis.

First, images acquired by the proposed method during the resin-impregnation process were converted into a binary image (Figure 4(a)). The HSL color plane was then extracted (Figure 4(b)) and converted to a binarized image by setting the threshold to the L plane (i.e. luminance). In the acquired void image, light was able to pass through the resin, the void (or air), and the impregnated glass fiber bundle, which therefore appear bright, whereas the gas–liquid interface, which is not transparent, appeared dark. Figure 5 shows an example of a luminance histogram of an image that includes voids. The histogram value h becomes large in the vicinity of brightness values of $i = 0$ and $i = 80$–170. The region near $i = 0$ indicates the black outline of the voids or the

Figure 2. Image of flow front during one-dimensional RTM.

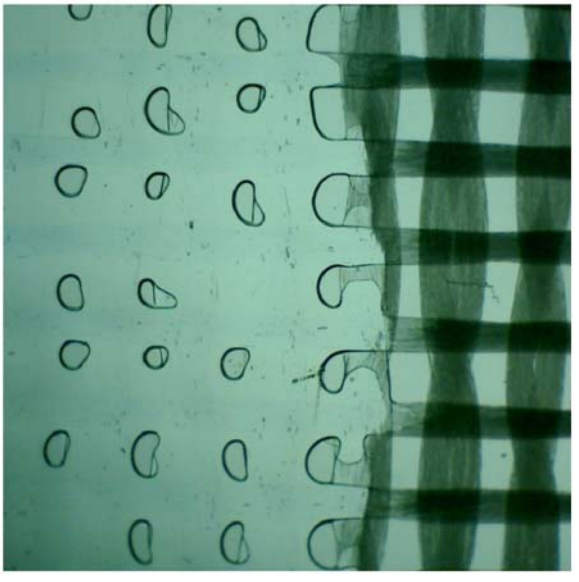

Figure 3. Microscopic image of flow front and voids observed by the proposed visualization method during RTM.

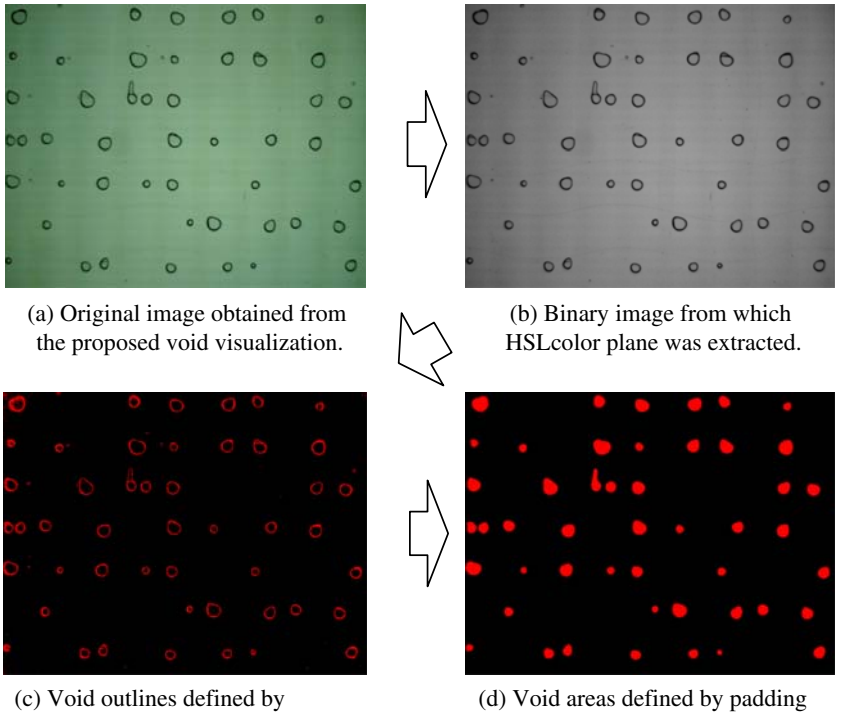

Figure 4. Flow chart of image analysis for measurement of void content.

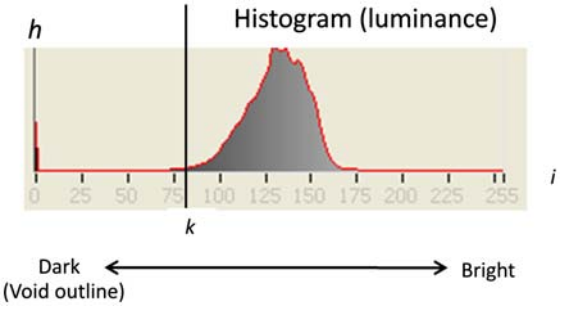

Figure 5. Histogram of the luminance extracted from the void distribution image. i is the gray-scale value (luminance), h is the histogram value, and k is the threshold value.

gas–liquid interface, whereas that near $i = 80$–170 indicates the other gray region. Therefore, by setting the threshold k such that it divides these two luminance peaks, we identified a void outline (Figure 4(c)). The area of each void was identified from the identified outlines of the voids by filling in the inside of the void outline. Finally, the small particles in the image, such as the dust contained in the resin, were removed by image filtering (Figure 4(d)). As a consequence, a region occupied by voids was identified, and the area of the void content could be calculated from the number of the pixels. It is assumed that the voids have a columnar shape because the fabric used in the experiments provided one layer, and its thickness was comparatively smaller than the diameter of the generated voids. Thus, the area contents of the voids were treated as their volume contents.

2.3. *Identification of resin flow velocity*

In the case of a one-dimensional flow, if we assume that a glass fabric is a homogeneous porous medium, the resin flow velocity U at a distance from the resin inlet x is represented as Equation (1) by Darcy's law.

$$U = -\frac{K}{\mu}\frac{\mathrm{d}P}{\mathrm{d}x} \tag{1}$$

here, K is the permeability in the flow direction, i.e. the longitudinal direction of the glass fabric, μ is the viscosity of the resin, and $\mathrm{d}P/\mathrm{d}x$ is the pressure gradient in the flow direction. Considering the incompressibility and quasi-static process of resin flow, the continuity equation is expressed as Equation (2).

$$\frac{\mathrm{d}U}{\mathrm{d}x} = 0 \tag{2}$$

by solving Equations (1) and (2) under the boundary condition $P = P_\mathrm{f}$ at $x = x_\mathrm{f}$ and $P = P_0$ at $x = 0$, where P_f is the pressure at the flow front and P_0 is the pressure at the resin inlet, we express the location of the flow front x_f at time t by the following equation.

$$t = \frac{\mu}{2K(P_0 - P_\mathrm{f})}x_\mathrm{f}^2 \tag{3}$$

from Equation (3), by recording the location of the flow front at selected time intervals during an experiment and by approximating using a quadratic function, we could determine the permeability K, which enables us to identify the flow front velocity at any point in the flow.

3. In situ measurement of void content during RTM

3.1. Experimental methods

The proposed method makes it possible to measure void contents just after air-trapping in their respective locations. In this way, using the proposed in situ void measurement method, we investigated the change in the void content distribution during one-dimensional RTM by comparing the void content measured at the point of air-trapping versus their content after resin curing.

A single layer of plain woven glass cloth (M100K104#110, Unitika glass fiber) was used as the glass fiber fabric, which had dimensions of 200 mm × 50 mm. The physical properties of the material are listed in Table 1. A curing agent (Epoch PN) was added at 1 PHR (per hundred resin) to the unsaturated polyester resin (Sundhoma PC184-C, DH material).

One-dimensional RTM experiments were carried out, as shown in Figure 1, while the negative pressure of a vacuum pump was kept constant at two separate rates of injection pressure, at 20 and 40 kPa, from the beginning of resin injection until the completion of resin curing. Note that the injection pressure indicates the differential pressure from the atmospheric pressure. The resin flow direction, i.e. the longitudinal direction, was parallel to the direction of the warp fiber of the fabric.

A digital microscope (M3, Scholar) was installed on the upper surface of the mold, and a photograph of the impregnation behavior at the flow front was taken by moving the microscope as the flow advanced. The measurement location was set at distances of $x = 50$, 75, 100, 125, 150, 175 mm from a resin inlet. The measurement area was set as a 5×15 mm rectangular area at each measurement location, where the longitudinal direction of the rectangular area was consistent with the direction perpendicular to resin flow. This is because in a one-dimensional flow, conditions such as flow velocity and pressure are constant along a direction perpendicular to the resin flow. After the completion of resin impregnation and curing, the same measurement area was again set

Table 1. Material property of glass fiber fabric.

Variable	M100K104#110
Thickness of fiber mat H [m]	1.4×10^{-4}
Superficial porosity of fiber mat Φ	0.18
Number of fiber bundles [25 mm]	19
Distance between bundles in warp direction L_{warp} [m]	4.1×10^{-4}
Distance between bundles in weft direction L_{weft} [m]	7.1×10^{-4}
Height of fiber bundle in warp direction h_{warp} [m]	8.4×10^{-5}
Height of fiber bundle in weft direction h_{weft} [m]	5.6×10^{-5}
Width of fiber bundle in warp direction w_{warp} [m]	5.9×10^{-4}
Width of fiber bundle in weft direction w_{weft} [m]	8.9×10^{-4}
Number of fiber inside bundles n	400
Porosity inside bundle ϕ	0.37
Fiber radius r [m]	4.2×10^{-6}

within view of the microscope. Note that it was assumed that a resin curing time of 24 h followed the completion of the impregnation.

The images obtained by the microscope at the point of air-trapping and after resin curing were processed and analyzed, as described in the Section 2.2, using image analysis software (Vision Assistant 8.5, National Instruments). The area ratio of the void content at each location was then calculated.

3.2. *Experimental results and discussion*

Figure 6 shows the relationship between the distance from the resin inlet x and the arrival time of the flow front t in each case for an injection pressure of 20 and 40 kPa. It was found that the arrival time of the resin at each location was shorter in the case of 40 kPa than that in the case of 20 kPa, and the relationship between the time and the location could be approximated using a quadratic function, which implies that the process of resin impregnation was in accordance with Darcy's law.

Figure 7 shows the flow front velocity of the resin at each location, as calculated by differentiating the approximation curve of the experimental results in Figure 6. As can be seen in the figure, at an injection of pressure of 40 kPa, the velocity of the resin flow front in each location is higher than that at an injection pressure of 20 kPa. This is because the pressure gradient at the same distance from the resin inlet becomes larger as the injection pressure becomes larger.

It is well known that a void shrinks because of an increase in pressure in the surrounding resin according to the advance of the flow front. To eliminate this effect, the void content measured after curing was converted to an adjusted value, assuming it was under the same pressure as it was at the point of air-trapping, by calculating the following state equation.

$$V_{v0} = \frac{P_v}{P_{v0}} V_v \tag{4}$$

where P_{v0} and V_{v0} are the initial inner pressure and the volume of the void at the point of void generation, respectively, whereas P_v and V_v are the inner pressure and the

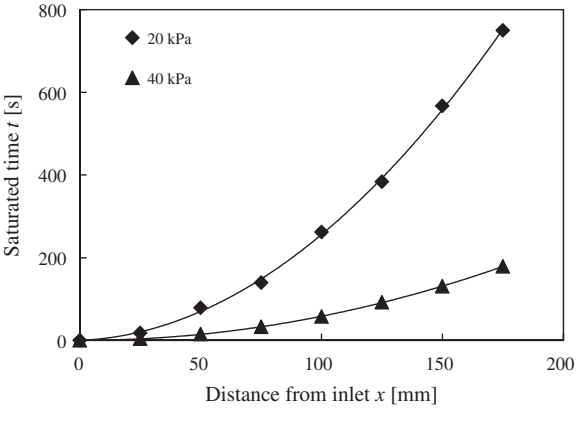

Figure 6. Flow front positions versus saturated time at injection pressures of 20 and 40 kPa. The plots were obtained from the experiments, and the curve fit was based on approximation using Darcy's law.

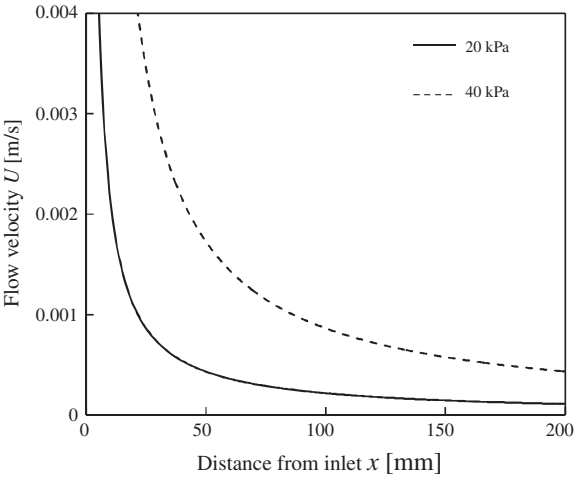

Figure 7. Resin flow velocity at each location derived from Darcy's law approximation of curve fit of the experimental data at injection pressures of 20 and 40 kPa.

volume of the void during measurement, respectively. Here, the temperature is assumed to be constant during the experiments.

Because the inner pressure of the void balances the pressure of the surrounding resin, the following Equation (5) is satisfied

$$P_{\mathrm{v}} = P_{\mathrm{r}} \tag{5}$$

where P_{r} is the pressure of the surrounding resin. The pressure of the surrounding resin at the completion of impregnation at each location x is obtained by uniting Darcy's law and a continuous equation and is expressed as Equation (6).

$$P_{\mathrm{r}} = P_0 + \frac{x}{x_{\max}}(P_{\mathrm{f}} - P_0) \tag{6}$$

where $x_{\max}$ is the final flow front distance that was attained, which corresponds to the entire length of the fabric.

Figure 8 shows the relationship between the distance from the resin inlet and the adjusted void content, as measured both at the point of air-trapping and after the resin has cured. In Figure 8, the void contents measured at both these locations increase as their distance from the resin inlet increases. This is because as the distance from the resin inlet increases, the resin flow velocity decreases, and the capillarity pressure becomes predominant; thus, a large void is formed between the fiber bundles owing to the prior resin flow inside the bundles, as shown in Figure 3. Moreover, a comparison between the two pressure conditions shows that the void content at 20 kPa is larger than that at 40 kPa, a result that is also attributed to the lower resin flow velocity.

When a comparison is made between at the point of air-trapping and after resin curing, an inversion phenomenon of the void content change was observed regardless of the injection pressure. That is, when the distance from the resin inlet is comparatively short, the void content decreases after resin curing, whereas when the distance is longer, the void content increases after resin curing.

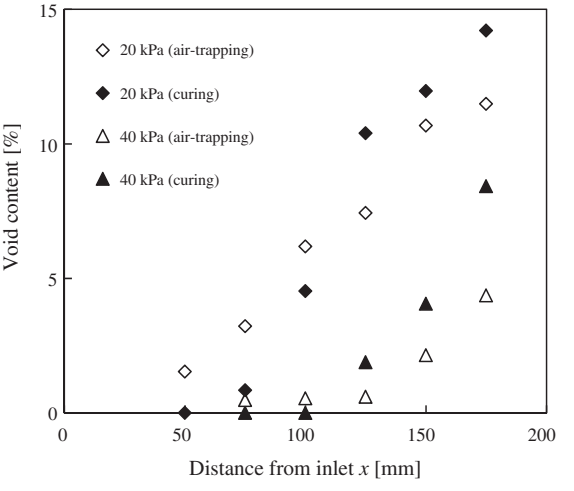

Figure 8. Void content at each location measured at the point of air-trapping and after curing at injection pressures of 20 and 40 kPa.

This finding can be explained by the ease with which the smaller void moves downstream. Figure 9 shows a model of a cross-section of the plain woven fabric. Owing to the undulation of the fiber bundle, there is space in the cross-section. When the formed void is smaller than this space, it is able to move downstream with the resin flow. Although the void is larger than the space, it is able to pass through the fiber bundle by shrinking in size when the following Equation is satisfied (7).[16]

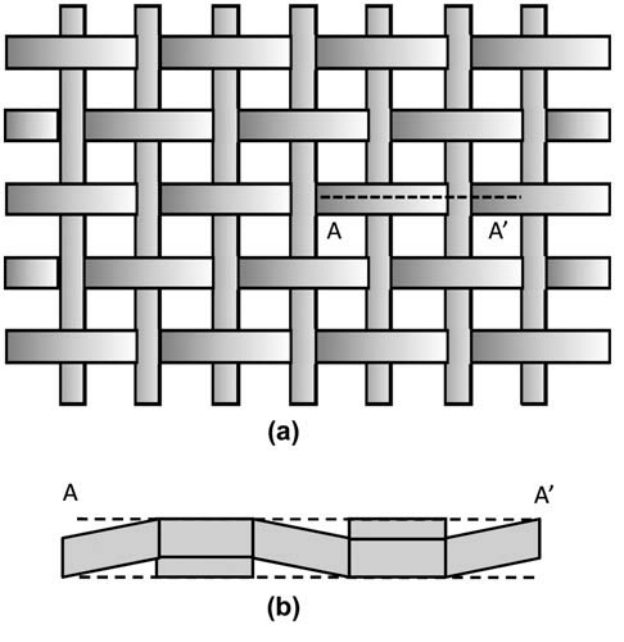

Figure 9. Inter-bundle porosity; (a) architecture of plain woven fabric and (b) a cross-section.

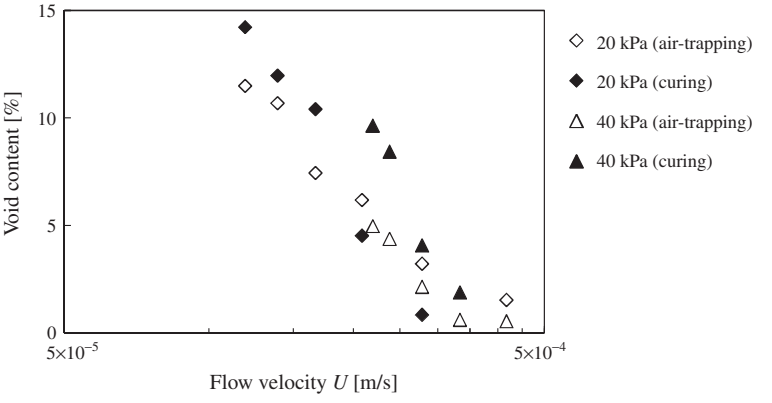

Figure 10. Relationship between flow velocity and void content measured at point of air-trapping and after curing.

$$\Delta p > \frac{\gamma_{lv}}{r}\left(1 - \frac{r}{r_v}\right) \tag{7}$$

here, Δp is the differential pressure that works back and forth within the fiber bundle, r denotes the diameters of the flow channel, r_v is the radius of the void, and γ_{lv} represents the tension at the gas–liquid interface. Otherwise, the movement of the void is interrupted by the presence of the fiber bundle, and it stays at the location where it was formed. Thus, it is easy for it to pass the bundle through when the diameter of the void is small. Therefore, since a trapped void is smaller as the distance from the inlet is shorter, the void moves downstream more easily, which results in a decrease in the void content within that short distance area. In the longer distance area, on the other hand, the larger void that was formed does not move easily and remains where it is. In addition, because the void flows from upstream, the measured void content increases due to the elapsed time.

Figure 10 shows the relationship between the resin flow velocity and the void content measured at the locations of air-trapping and after resin curing. The flow velocity was calculated from the relationship between the flow velocity and the location, as shown in Figure 7. It was found that the void contents at the point of air-trapping are almost the same at the same flow velocity for the different injection pressures. The void content after the resin cure, however, varies from that at the point of air-trapping, and this difference increases as the injection pressure increases. Thus, the void content after resin curing depends on the pressure, in addition to the flow velocity, i.e. the pressure gradient. Because this phenomenon cannot be explained by Equation (7), we address the mechanism in detail in the next section.

4. Change in void contents with elapsed time

4.1. Experimental methods

To investigate the mechanism that causes a difference between the void content as measured at the point of air-trapping versus after resin curing, we measured the time-elapsed change in the void content between these two points by fixing the position of the microscope. Measurements were taken at distances of $x = 100$ and 150 mm from the resin inlet, at an injection pressure of 40 kPa. The experimental setup, the fabric, the

resin, and the method used to measure the void content using image analysis were the same as in the experiments described in Section 3.

4.2. Experimental results and discussion

Figure 11(a) and (b) show the void content from the point of air-trapping until resin curing at distances of $x = 100$ and 150 mm from the resin inlet, respectively. The abscissa indicates the elapsed time where $t = 0$ indicates the point of air-trapping, and ∞ indicates the cured states, corresponding to about 24 h after the air-trapping. The t_{fill} indicates the time when the resin impregnation is complete in the entire area, and t_{gel} is the time when gel formation begins, based on observation of the resin in the other resin container. The ordinate is the void content, which was standardized by using the void content at $t = 0$. The curved line indicates the shrinkage of the void due to the resin pressure change according to the advance of the flow front, as predicted by Equation (4).

In the cases of both $x = 100$ and 150 mm, the void content decreased until $t = t_{fill}$, and then, increased as time elapsed. However, its rate of increase decreased after $t = t_{fill}$, after which it became almost constant. The void content at $t = \infty$ became slightly smaller than that at $t = 0$ in the case of $x = 100$ mm, whereas it became larger than that at $t = 0$ in the case of $x = 150$ mm. An inversion phenomenon, as shown in Figure 8, was also observed, in which the void content decreases with elapsed time at a short distance and increases at a longer distance.

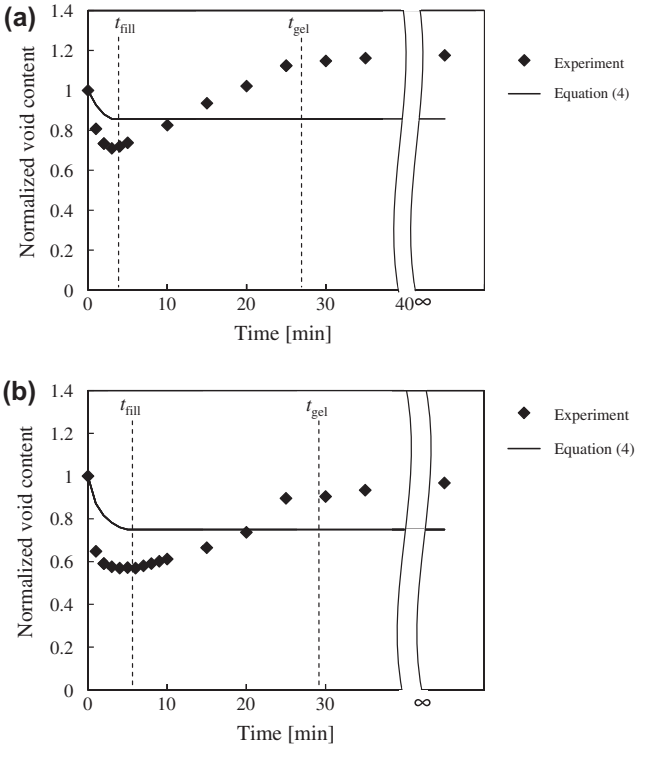

Figure 11. Change in void content from point of air-trapping until resin curing at an injection pressure of 40 kPa at (a) $x = 100$ mm and (b) $x = 150$ mm.

To investigate the void change mechanism, taking into consideration the results of microscopic observation, the experimental results were divided into three steps: (i) $t = 0 - t_{\text{fill}}$, (ii) $t = t_{\text{fill}} - t_{\text{gel}}$, and (iii) $t = t_{\text{gel}} - \infty$.

(i) $t = 0 - t_{\text{fill}}$

The void content decreased as time elapsed, although its ratio of change gradually became small, and the content was constant at around $t = t_{\text{fill}}$. Although this decrease in void content is partially due to the void shrinkage caused by the surrounding pressure change, the amount of the decrease in void content exceeds the model prediction. The decrease in the ratio of the void at $x = 100$ mm was larger than that at $x = 150$ mm.

From microscopic observation, it was verified that after the flow front passed, the downstream movement of the trapped voids could be observed, as shown in Figure 12. Moreover, the voids generated inside the fiber bundle also flowed outside the fiber bundle, as shown in Figure 13. This behavior occurred intermittently within the range of $t = 0 - t_{\text{fill}}$, and these voids moved downstream and stayed between the fiber bundles closer to the flow front or were integrated into other voids.

This finding verifies the fact that the decrease in void content was caused not just by shrinkage due to pressure change but also by the downstream movement with the resin flow or that the voids disappeared upon reaching the flow front. The decrease in void content at $x = 100$ mm was larger than that at $x = 150$ mm because of the fact that void movement took place more easily at $x = 100$ mm, as the pressure gradient was larger and the size of the voids was comparatively small.

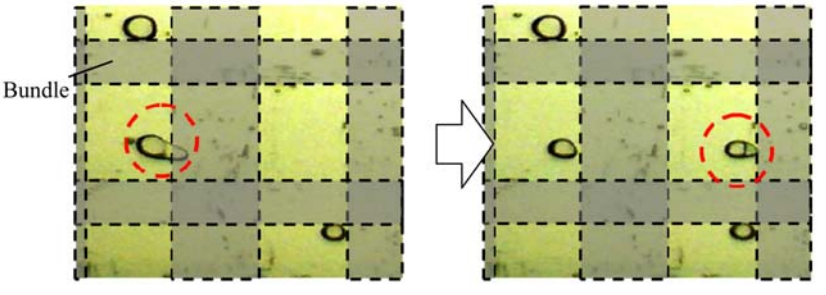

Figure 12. Void transportation through a fiber bundle downstream with resin flow.

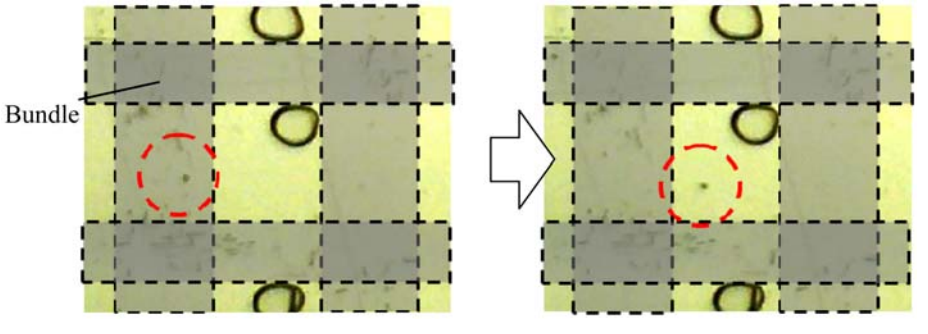

Figure 13. Transportation of intra-bundle void to outside of a bundle.

(ii) $t = t_{\text{fill}} - t_{\text{gel}}$

Based on the void shrinkage model that uses the state equation, when the advance of the flow front stops, the surrounding pressure does not change; thus, it is expected that the shrinkage of the void will also stop. However, the void content increased after the resin impregnation was complete $(t = t_{\text{fill}})$.

Based on the results of microscopic observation, the void expanded without integration into other voids as the time elapsed after $t = t_{\text{fill}}$, as shown in Figure 14. This may be the result of molecular diffusion at the interface between the void and the resin, which could follow two models: (1) if the gas molecule inside the void diffuses into the resin, the void will shrink or dissolve, and (2) if the gas dissolved in the resin diffuses into the void, the void will expand. When the void is assumed to be globular, the change in the void's volume due to molecular diffusion is expressed by Equation (8).[18,19]

$$\frac{\mathrm{d}R}{\mathrm{d}t} = -\frac{D(C_{\mathrm{s}} - C_{\infty})}{\rho R}\left[1 + \frac{R}{(\pi D t)^{1/2}}\right] \tag{8}$$

here, R is the void radius, D is the diffusion factor, C_{s} is the saturation solubility of the gas into the resin, C_{∞} is the initial solubility of the gas into the resin, and ρ is the gaseous density in the void. From Equation (8), it can be said that the shrinkage or expansion of the void due to molecular diffusion depends on whether $C_{\mathrm{s}} - C_{\infty}$ is positive or negative, i.e. whether the resin is undersaturated or supersaturated with the gas, respectively. The saturation solubility C_{s} of the gas into the resin follows Henry's law in Equation (9).[18,19]

$$C_{\mathrm{s}} = HP \tag{9}$$

where H is the constant and P is the pressure of the resin. In the present study, resin injection was conducted by applying negative pressure using a vacuum pump at the outlet as a VaRTM process. Therefore, the pressure of the resin during impregnation was below the atmospheric pressure. The saturation solubility of the gas into the resin becomes small during impregnation as compared with the state that is preserved under atmospheric pressure. Thus, the resin becomes supersaturated, and the gas molecule dissolved in the resin diffuses into the void, causing the void to expand after $t = t_{\text{fill}}$.

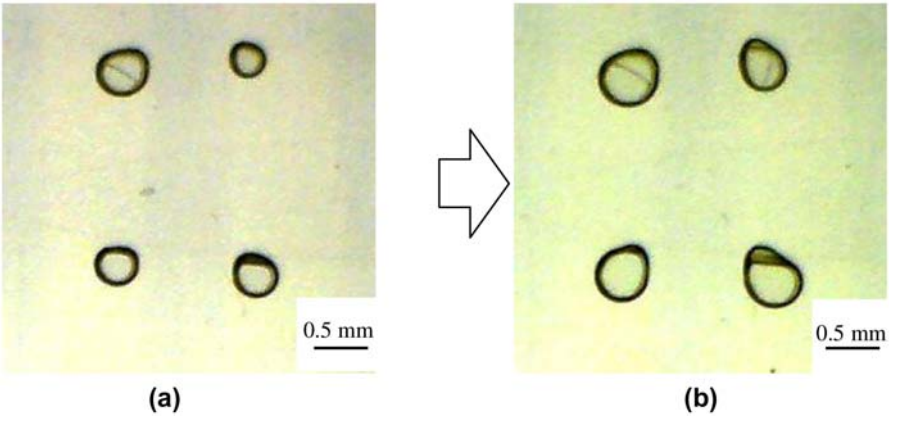

Figure 14. Void growth as time elapses during RTM; (a) 5 min after void formation and (b) 25 min after void formation.

The behavior in which the amount of voids increases with an increase in elapsed time as the resin injection pressure becomes higher, as mentioned in Section 3.2, can be explained by the molecular diffusion. The lower pressure P (or the higher injection differential pressure in VaRTM) indicates a lower C_s from Equation (9), which results in a larger void increase from Equation (8). Under a constant injection pressure, the longer distance area indicates a lower pressure at $t = t_{fill}$, which results in a larger void increase due to the diffusion. Thus, the molecular diffusion is also attributed to the inversion phenomena mentioned in Section 3.2. However, the molecular diffusion alone cannot explain the void decrease in the short distance area. Therefore, both the void movements and the molecular diffusion are responsible for the inversion phenomenon.

The diffusion of the gas molecule to the void may also occur during $t = 0 - t_{fill}$. However, because the effects of the void movement and shrinkage due to the surrounding pressure change are larger than the effects due to diffusion, the void content does not increase.

(iii) $t = t_{gel} - \infty$

After the beginning of the resin cure or gelation process, the void content does not change significantly. This implies that the cure shrinkage does not have a significant influence on the variation in void content. Moreover, diffusion from a solid to a gas takes place extremely late as compared to the diffusion from a liquid to a gas. Thus, the change in void content due to molecular diffusion hardly takes place at this stage.

To summarize, the process in which void content changes after void formation is as follows. The void moves along with the resin flow, escapes from fiber bundles to the space between the bundles, shrinks because of the surrounding pressure change, and expands because of the molecular diffusion at the gas–liquid interface. The influence of each factor in this process differs according to the resin injection pressure and the location where measurements are taken, i.e. the pressure gradient.

In the present study, we used one-layer fabrics to focus on void formation due to woven fabric architecture in more detail. Note that factors other than the fabric architecture may still have had an effect, such as wettability between the resin and mold or the gap between the mold and fabrics. To assess these effects properly and model the void entrapment between multiple layers, we will conduct the same in situ void measurements using multilayer fabrics in future work.

5. Conclusions

An in situ method for measuring void content during resin impregnation was created by combining image analysis with visualization technique of the resin flow and void generation during one-dimensional RTM. Using the proposed method, we measured the changes in the distribution of the void content at the point of air-trapping and after resin curing. In the results, an inversion phenomenon was observed in which the void content decreased with elapsed time at a short distance from the resin inlet, but increased at a longer distance. This difference can be explained by the relative ease with which the void could move at a shorter distance and the effect of molecular diffusion.

In addition, by measuring the change in void content over the time that elapsed from the point of air-trapping until resin curing, the following observations were made:

(1) The void content decreases from the point of air-trapping to the completion of impregnation because of the change in the surrounding pressure and the

movement of the void through the fiber bundles. The ratio of its decrease is larger for a higher pressure gradient (or a faster flow velocity).

(2) The void content increases from the completion of impregnation to the point of resin gelation because of molecular diffusion. The ratio of this increase is larger at a higher injection pressure in the case of VaRTM.

(3) From the point of gelation to the point of curing, the influence of the cure shrinkage and of the molecular diffusion from a solid to a gas is small; thus, there is hardly any change in the void content.

References

[1] Kruckenberg T, Paton R. Resin transfer moulding for aerospace structures. Dordrecht (The Netherlands): Springer; 1998.

[2] Matsuzaki R, Kobayashi S, Todoroki A, Mizutani Y. Control of resin flow/temperature using multifunctional interdigital electrode array film during a vartm process. Compos. Part A: Appl. Sci. Manuf. 2011;42:782–793.

[3] Matsuzaki R, Kobayashi S, Todoroki A, Mizutani Y. Full-field monitoring of resin flow using an area-sensor array in a vartm process. Compos. Part A: Appl. Sci. Manuf. 2011;42: 550–559.

[4] Patel N, Lee LJ. Effects of fiber mat architecture on void formation and removal in liquid composite molding. Polym. Compos. 1995;16:386–399.

[5] Rohatgi V, Patel N, Lee LJ. Experimental investigation of flow-induced microvoids during impregnation of unidirectional stitched fiberglass mat. Polym. Compos. 1996;17:161–170.

[6] Moon Koo Kang, Woo Il Lee, Thomas Hahn H. Formation of microvoids during resin-transfer molding process. Compos. Sci. Technol. 2000;60:2427–2434.

[7] Lundström TS, Gebart BR. Influence from process parameters on void formation in resin transfer molding. Polym. Compos. 1994;15:25–33.

[8] Huang H, Talreja R. Effects of void geometry on elastic properties of unidirectional fiber reinforced composites. Compos. Sci. Technol. 2005;65:1964–1981.

[9] Varna J, Joffe R, Berglund LA, Lundström TS. Effect of voids on failure mechanisms in RTM laminates. Compos. Sci. Technol. 1995;53:241–249.

[10] Ghiorse SR. Effect of void content on the mechanical properties of carbon/epoxy laminates. SAMPE Q. 1993;24:54–59.

[11] Testing methods for carbon fiber content and void content of carbon fiber reinforced plastics. JIS K 7075.

[12] Patel N, Rohatgi V, Lee LJ. Micro scale flow behavior and void formation mechanism during impregnation through a unidirectional stitched fiberglass mat. Polym. Eng. Sci. 1995;35:837–851.

[13] Leclerc JS, Ruiz E. Porosity reduction using optimized flow velocity in Resin Transfer Molding. Compos. Part A: Appl. Sci. Manuf. 2008;39:1859–1868.

[14] Schell JSU, Deleglise M, Binetruy C, Krawczak P, Ermanni P. Numerical prediction and experimental characterisation of meso-scale-voids in liquid composite moulding. Compos. Part A: Appl. Sci. Manuf. 2007;38:2460–2470.

[15] Frishfelds V, Lundström TS, Jakovics A. Bubble motion through non-crimp fabrics during composites manufacturing. Compos. Part A: Appl. Sci. Manuf. 2008;39:243–251.

[16] Lundström TS. Bubble transport through constricted capillary tubes with application to resin transfer molding. Polym. Compos. 1996;17:770–779.

[17] LundströmTS. Measurement of void collapse during resin transfer moulding. Compos. Part A: Appl. Sci. Manuf. 1996;28:201–214.

[18] Jonathan R, Wood MGB. Void control for polymer-matrix composites (1): theoretical and experimental methods for determining the growth and collapse of gas bubbles. Compos. Manuf. 1994;5:139–147.

[19] Jonathan R, Wood MGB. Void control for polymer-matrix composites (2): theoretical and experimental methods for determining the growth and collapse of gas bubbles. Compos. Manuf. 1994;5:149–158.